

# EVOLUTION OF PLANETS IN DISKS

Wilhelm Kley

Institut für Astronomie & Astrophysik, Abt. Computational Physics, Universität Tübingen,  
Auf der Morgenstelle 10, D-72076 Tübingen, Germany

## ABSTRACT

The main properties of the observed extrasolar planets are reviewed with respect to their relevance to the formation scenario of planetary systems. Results of numerical computations of embedded planets in viscously evolving disks are presented. Emphasis is given to the accretion and migration process. New calculations on inviscid disks are shown.

The second part of the talk concentrates on resonant planetary systems. Among the observed extrasolar systems there are 3 confirmed cases, Gl 876, HD 82943 and 55 Cnc, where the planets orbit their central star in a low order mean motion resonance. Results of numerical simulations modeling the formation and evolution of such systems are presented.

Key words: planet formation, numerical hydrodynamics, resonant orbits.

## 1. OBSERVATIONS

Since the first discovery of extrasolar planets around main sequence stars in 1995, their number has risen to over 100 planets today. For an always up-to-date list see e.g. <http://www.obspm.fr/encycl/encycl.html>, maintained by J. Schneider. Apart from two discoveries by the transit method of OGLE-objects (Konacki et al. 2003; Dreizler et al. 2003), all others have been found by radial velocity measurements. Among all systems, there are at least 12 planetary systems with two or more planets; a summary of their properties has recently been given by Marcy et al. (2003). Longer observations to study trends in velocity curves may still increase this number. Of all stars investigated, planets have been found so far around about 7 %.

The orbital properties of these planetary systems display features quite different from those of our own solar system. Some statistical properties are summarized in Mazeh & Zucker (2002), Santos et al. (2003) and additional data may be obtained from

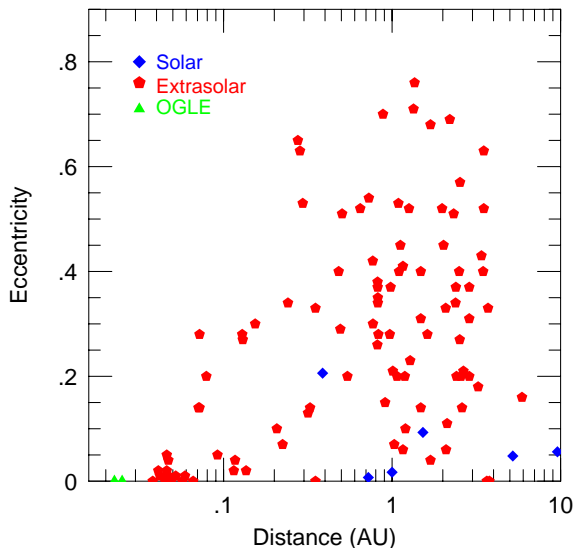


Figure 1. Eccentricity vs. distance for the extrasolar planets. For comparison the solar system planets and the two OGLE objects are also included.

<http://www.obspm.fr/encycl/encycl.html>. As an example we display in Fig.1 the eccentricity versus mass distribution of all planets detected so far. While the planets close to the star (hot Jupiters) tend to have circular orbits due to tidal circularization the planets further out have a rather broad eccentricity distribution which is essentially indistinguishable from that of binary stars. Additionally, the cumulative eccentricity-period distribution of stellar binaries and planetary systems are also nearly identical for periods larger than about 10 days (Mazeh & Zucker 2002). This may imply a common origin of the eccentricities, caused for example by dynamical gravitational interaction.

A summary of the main properties of the exoplanets is outlined in the following. The reasons why those characteristics present problems to the standard planet formation scenarios, is given just below the individual points, see also Lissauer (2002).

- Large Masses ( $0.2\text{--}17 M_{\text{Jup}}$ )

Tidal interaction between the planet and the protoplanetary disk results for planets larger than about 1 Jupiter mass ( $M_{Jup}$ ) in the creation of a density gap in the disk (Lin & Papaloizou 1980, 1993). In turn, this gap will reduce the accretion onto the planet and limit the mass to about  $1 M_{Jup}$ , just as in our solar system (Lissauer 1993).

- **Small Distance (0.04 - 3.3 AU)**  
The high disk temperature in the vicinity of the star makes it difficult to allow for condensation of solid material. Thus, the cores of the protoplanets are expected to have been formed beyond the so called snow line at a distance of about 3 AU and larger from the star (Sasselov & Lecar 2000).
- **Large Eccentricities (0.0 - 0.91)**  
It is usually assumed that planets form in a protoplanetary disk, which is essentially in a Keplerian rotation around the star. Hence, directly after formation, planets are expected to orbit on circular orbits.
- **Resonant Orbits (2:1, 3:1)**  
The condensation process in the disk and the subsequent oligarchic (Kokubo & Ida 1998; Thommes et al. 2003) growth of planetesimals towards larger planets can occur theoretically at arbitrary orbits. For stability reasons, only the planets cannot be on orbits separated by less than about 10 Hill radii.
- **Free Floaters (in Jupiter-mass range)**  
Recently, objects in the planetary mass range (a few  $M_{Jup}$ ) but not orbiting stars have been found (Lucas & Roche 2000; Béjar et al. 2001). Although not directly part of a planetary system today, the origin of these objects may be related to planet formation, followed by ejection processes. It is believed that bodies of a few  $M_{Jup}$  are too small to have formed by direct gravitational collapse.

All the raised features may have their origin in an evolution process of the young planets still embedded with the protoplanetary disk from which they formed originally.

## 2. MODELING EMBEDDED PLANETS

We shall focus here in the joint evolution of planets and disks, and concentrate on the fully non-linear hydrodynamical calculations. In recent years several simulations have been performed (Kley 1999; Bryden et al. 1999; Lubow et al. 1999; Nelson et al. 2000; D'Angelo et al. 2002). In the following we describe how these calculation typically proceed.

All models consider essentially only the late stages of the planet formation scenario. It is assumed that protoplanets have already been formed for example

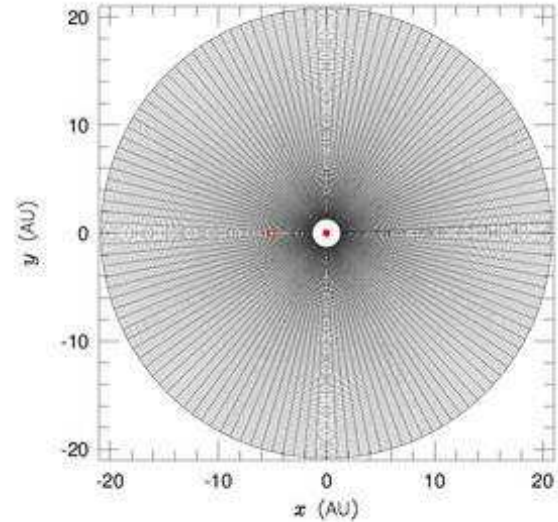


Figure 2. A typical computational grid-system ( $128 \times 128$ ) used in planet-disk computations

by core accretion. The subsequent evolution of the embedded planets is studied considering the mutual gravitational interaction between disk and planets. In this contribution we shall focus on the purely hydrodynamic evolution, as elsewhere in this volume Richard Nelson describes magnetic effects as well.

The ingredients of a model for embedded planets consists of a star (of typical one solar mass,  $1 M_{\odot}$ ), a protoplanetary disk ( $M_{disk} = 0.01 M_{\odot}$ ), and a given number of planets.

The disk is modeled by a hydrodynamical evolution in the field of the star and the planets. It is assumed to be geometrically thin with a small vertical thickness  $H/r \ll 1$ . Mostly it has been modeled by a two-dimensional approximation in  $r - \varphi$ -coordinates (Kley 1999; Bryden et al. 1999; Lubow et al. 1999; Nelson et al. 2000; D'Angelo et al. 2002). However recently, also fully three dimensional models ( $r, \varphi, \vartheta$ ) have been performed (Kley et al. 2001; D'Angelo et al. 2003; Bate et al. 2003). To capture all relevant effects global models of the disk extending typically from about 1 to 30 AU or more have to be invoked. Initial density profiles typically have power laws for the surface density  $\Sigma \propto r^{-s}$  with  $s$  between 0.5 and 1.5. Nearly all published models have a fixed radial temperature distribution. Mostly, the aspect ratio  $H/r$  is held constant in the disk. From there the temperature profile follows  $T(r) \propto r^{-1}$ . In three dimensional models the temperature is vertically constant and the density  $\rho$  follows a Gaussian.

For the anomalous viscosity a Reynolds stress tensor formulation (Kley 1999) is used where the kinematic viscosity  $\nu$  is either constant or given by an  $\alpha$ -prescription  $\nu = \alpha c_s H$ , where  $\alpha$  is constant and  $c_s$  is the local sound speed. From observations, values lying between 0.001 and 0.01 are inferred for the  $\alpha$ -parameter. Full MHD-calculations have

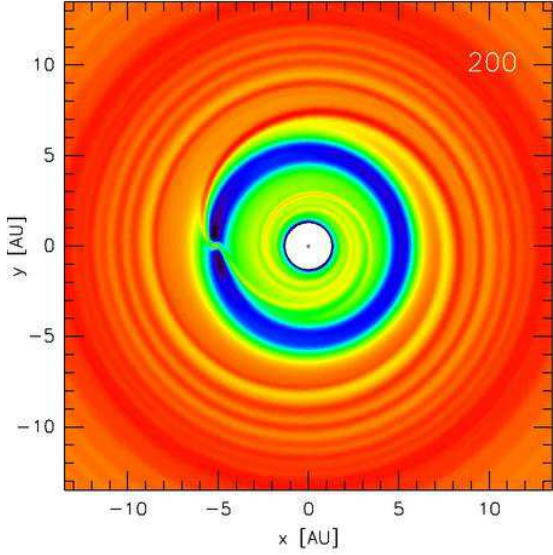


Figure 3. Surface density profile for an initially axisymmetric planet-disk model after 200 hundred orbital orbits of the planet.

shown that the viscous stress-tensor ansatz may give (for sufficiently long time averages) a reasonable approximation to the mean flow in a turbulent disk (Papaloizou & Nelson 2003).

The embedded planets are assumed to be point masses (using a smoothed potential), and together with the star they are treated as classical N-body system. The disk also influences the orbits through the gravitational torques. This is the desired effect to be studied which will cause the orbital evolution of the planets. The planets may also accrete mass from the surrounding disk.

The initial conditions of the disk are axisymmetric with some given profile for  $\Sigma(r)$  and  $T(r)$  as outlined above. Then a Jupiter type planet is placed into this disk at a distance of several AU (eg. 5.2), and the joint evolution of the (hydrodynamic) disk and the planetary (N-body) system is then followed through numerical integration. In this review we shall not give any details on the numerical issues, and refer the reader to the appropriate literature (Kley 1998, 1999; Bryden et al. 1999). Just to give some impression of how a typical (low-resolution) grid system looks like we display in Fig.2 the  $r - \varphi$  grid having a resolution of  $128 \times 128$  gridcells. The radial coordinate extends from 1.3 AU up to 20 AU. For illustration the star is indicated by central dot and the Roche-lobe of a  $1 M_{Jup}$  planet by the solid line around the planetary position  $x_p = -5.2, y_p = 0$ . As can be seen, at this resolution the Roche-lobe of the planet is merely resolved by a few grid-cells.

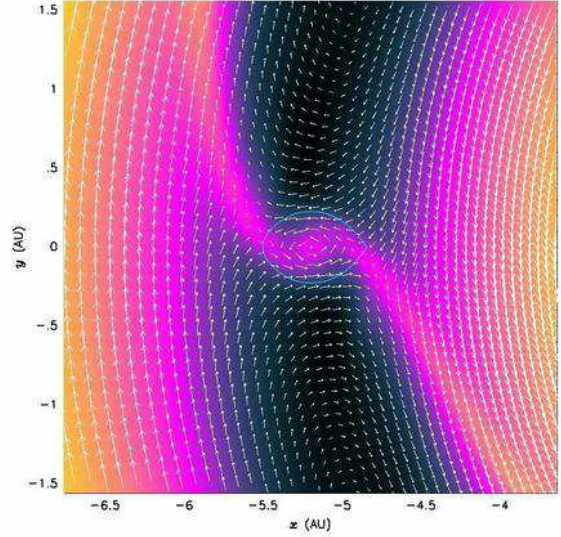


Figure 4. Surface density and velocity arrows for a one Jupiter mass model.

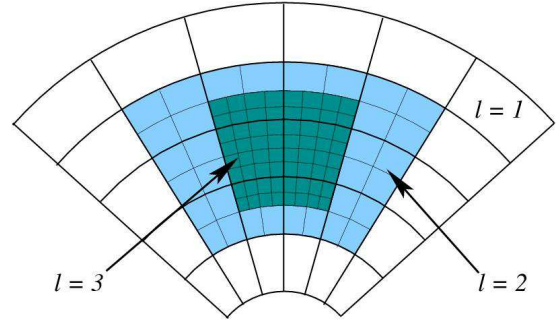


Figure 5. Structure of a nested grid centered on the planet. Three levels of grids are shown (from D'Angelo et al. (2002)).

### 3. VISCOUS LAMINAR DISKS

The type of modeling outlined in the previous section yields in general smooth density and velocity profiles, and we refer to those models as *viscous laminar disk* models. In contrast to models which do not assume an a priori given viscosity and rather model the turbulent flow directly.

#### 3.1. The global view

A typical result of such a viscous computation obtained with a  $128 \times 280$  grid is displayed in Fig.3. Here, the planet with mass  $M_p = 1M_{Jup}$  and semi-major axis  $a_p = 5.2\text{AU}$  is *not* allowed to move and remains on a fixed circular orbit. The disk has  $H/r = 0.01$  and  $\nu = 10^{-5}$  in units of  $a_p^2 \Omega_p$ , where  $\Omega_p$  is the orbital Keplerian frequency of the planet. This viscosity for the given temperature is equivalent to  $\alpha = 4 \cdot 10^{-3}$  at the location of the planet. Clearly seen are the major effects an embedded planet has on the protoplanetary accretion disk. The gravitational



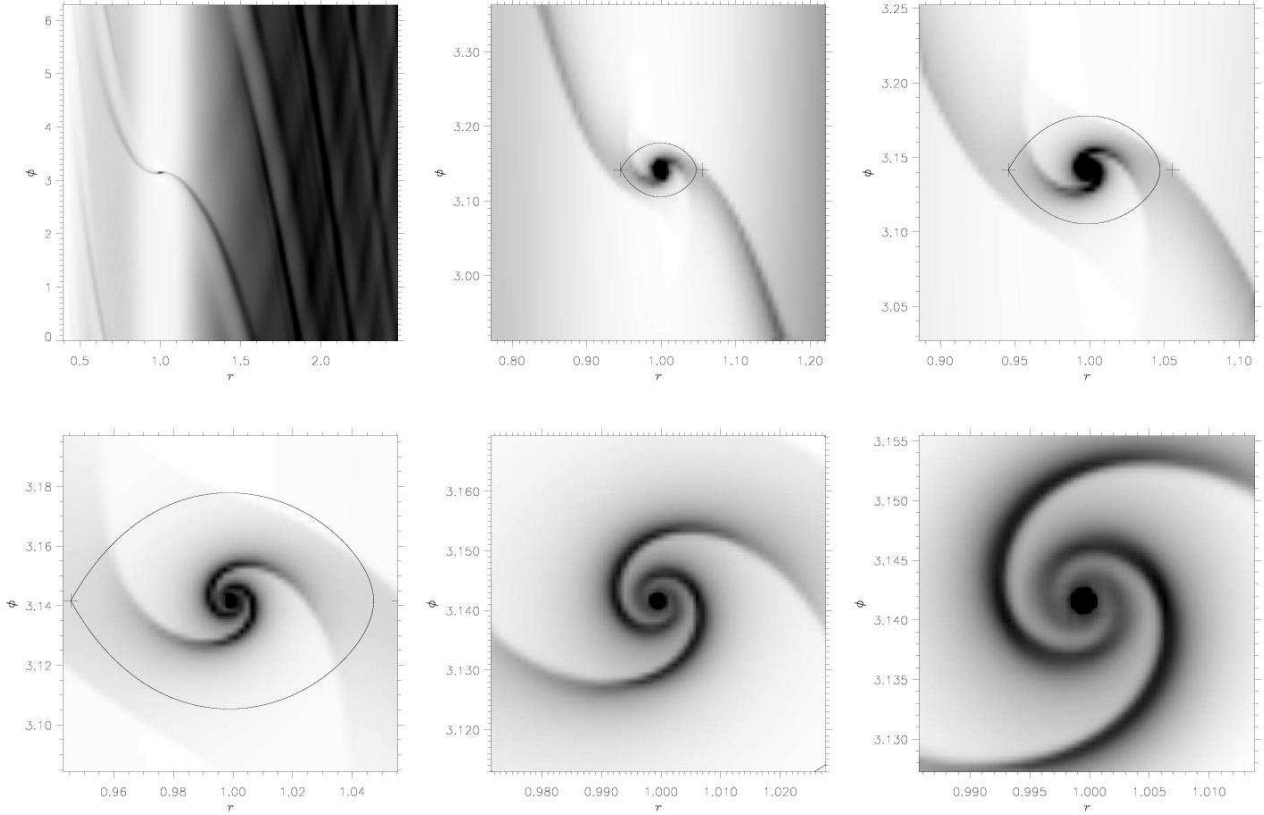


Figure 6. Density Structure of a  $1M_{Jup}$  on each level of the nested grid system, consisting of 6 grid levels in total.

force of the planet leads to spiral wave pattern in the disk. In the present calculation (Fig.3) there are two spirals in the outer disk in the inner disk. The tightness of the spiral arms depends on the temperature (i.e.  $H/r$ ) of the disk. The smaller the temperature the tighter the spirals. The second prominent feature is the density gap at the location of the planet. It is caused by the deposit of positive (at larger radii) and negative (at smaller radii) angular momentum in the disk. The spiral waves are corotating in the frame of the planet, and hence their pattern speed is faster (outside) and lower (inside) than the disk material. Dissipation by shocks or viscosity leads to the deposit of angular momentum, and pushes material away from the planet. The equilibrium width of the gap is determined by the balance of gap-closing viscous and pressure forces and gap-opening gravitational torques. For typical parameter of a protoplanetary disk, a Saturn mass planet will begin to open a visible gap.

The density structure and flow field in the vicinity of the planet for such a model with the same physical parameter but a resolution of  $128 \times 440$  grid-cells, is displayed in Fig.4. The solid line represents the size of the Roche-lobe of the planet. The velocity arrows are calculated with respect to the planet in the corotating frame. At this resolution the Roche-lobe is still barely resolved and the rotation of the material around the planet is visible. It is noticeable that

even for a one Jupiter mass planet with a very deep gap, mass accretion is still possible. Only beyond about  $5 M_{Jup}$  the gap gets to wide and additional accretion is strongly inhibited.

### 3.2. The local view

To obtain more insight into the flow near the planet and to calculate accurately the torques of the disk acting on the planet, a much higher spatial resolution is required. As this is necessary only in the immediate surrounding of the planet, a number of nested-grid and also variable grid-size simulations have been performed (D'Angelo et al. 2002, 2003; Bate et al. 2003). As an example we display in Fig.5 the structure of such a nested grid system with three levels. The equations are solved on all levels and appropriate boundary conditions are formulated to ensure mass, energy and angular momentum conservation across the grids. This type of grid-system is not adaptive, as it is defined in the beginning and does not change with time. The planet is placed in the center of the finest grid.

The result for a 2D computation using 6 grids is displayed in Fig.6, for more details see also D'Angelo et al. (2002). The top left base grid has a resolution of  $128 \times 440$  and each sub-grid has a size of  $64 \times 64$  with a refinement factor of two from level

to level. It is noticeable that the spiral arms inside the Roche-lobe of the planet are detached from the global outer spirals. The two-armed spiral around the planet extends deep inside the Roche-lobe and allow for the accretion of material onto the planet. The nested-grid calculations have recently been extended to three dimensions (3D) and a whole range of planetary masses have been investigated, starting from 1 Earth mass to a few Jupiter masses (D'Angelo et al. 2003). In the 3D case the strength of the spiral arms are weaker and accretion occurs primarily from regions above and below the midplane of the disk.

### 3.3. Accretion and Migration

These high-resolution numerical computations allow for a detailed computation of the torque exerted by the disk material onto the planet, and its mass accretion rates. Fig.7 gives the inverse  $1/\tau_M$  of the migration for three dimensional nested grid calculations as a function of the planet mass, given in units of the mass of the central star,  $q = M_p/M_\odot$ . The upper dark solid line represents an analytical two-dimensional linear estimate by Ward (1997) and the lower straight line by Tanaka et al. (2002), which assumes a three-dimensional flow and takes the corotation torques into account. The symbols refer to different approximations of the potential of the planet. It can be seen that for low masses  $q \approx 10^{-5}$  and intermediate masses  $q \approx 8 \cdot 10^{-5}$  the numerical results fit well to the linear theory. In the intermediate range of about  $q \approx 3 \cdot 10^{-5}$  the migration rates are about an order of magnitude longer (D'Angelo et al. 2003). This effect may be caused by the onset of gap formation in the mass range of about 10-15 earth masses. Here nonlinear effects begin to set in and modify the physics. These results should be compared to those obtained by Bate et al. (2003).

The consequences of accretion and migration have been studied by numerical computations which do not hold the planet fixed at some radius but rather follow the orbital evolution of the planet (Nelson et al. 2000). In Fig.8 we display the radial evolution of an embedded protoplanet as it evolves with the disk. The typical migrations timescales are found to be of the order  $10^5$  yrs, while the accretion timescale may be slightly smaller. When planets reach the vicinity of the central star they can reach up to about  $4 M_{Jup}$ .

## 4. INVISCID DISKS

To investigate the influence of viscosity we studied recently also inviscid models with no physical viscosity added. Only a numerical bulk viscosity has to be added to ensure numerical stability Kley (1999). However, this has no influence on the physical effects of the simulations. In Fig.9 we display the density structure of such an inviscid model for a  $1 M_{Jup}$  planet. The planet is not

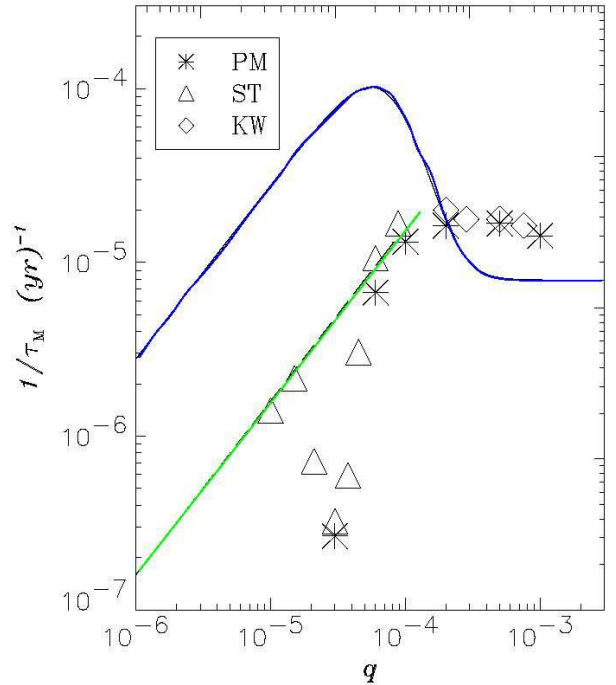


Figure 7. The inverse of the migration rate for different planet masses. The symbols denote different approximations (smoothing) for the potential of the planet.

allowed to move and for stability purposes its mass is gradually switched on during the first 5 orbits. Results are displayed at 4 different times (5, 10, 15, 32). After only 5 orbits the spiral waves are already clearly visible, as they form on a dynamical time scale. The gap is just beginning to clear. At the edges of the gap high density blobs (*vortices*) are forming which are reduced in number through merging. Eventually only one big blob remains. Also inside the gap, some detailed structure is visible. In comparison, fully viscous simulation show these vortices mostly as transient features in the beginning of the simulations. They vanish later on as a result of the viscosity. If accretion and also migration of the planet is considered, these moving vortices may create some more complex time dependence. However, the details of such inviscid models will have to be studied in future work. Vortices in accretion disks have sometimes been considered to enhance planet formation either through triggering a direct gravitational instability or by trapping particles in it Godon & Livio (2000); de la Fuente Marcos & Barge (2001); Klahr & Bodenheimer (2003).

## 5. RESONANT SYSTEMS

In this part we would like to concentrate on planetary systems which are in resonance. The above mentioned hydrodynamic simulations with single planets have been extended to models which contain multiple planets. It has been shown (Kley 2000; Bryden et al.

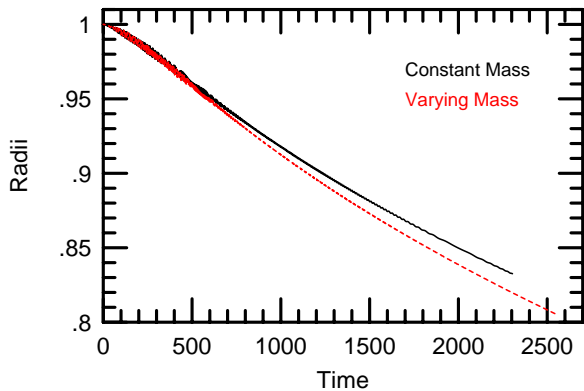


Figure 8. The radial position of an initially  $1M_{Jup}$  planet evolving with the disk. In one of the cases the mass was held fixed while in the other mass accretion from the disk was taken into account.

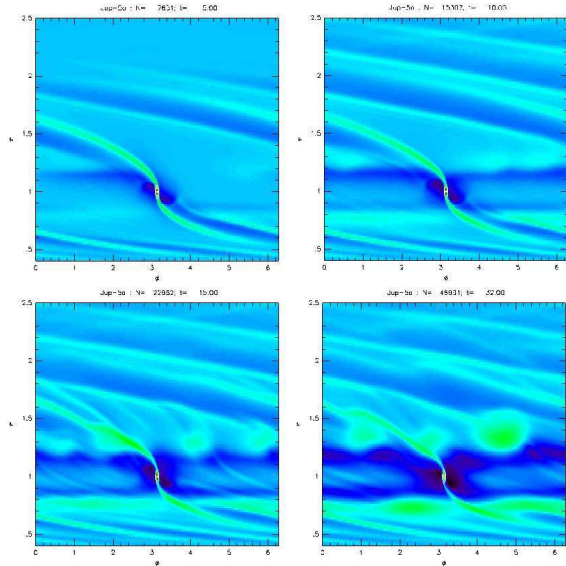


Figure 9. Results of an inviscid disk computation with an embedded  $1 M_{Jup}$  planet. Results are displayed at four different times (5, 10, 15, and 32) in units of the orbital period of the planet. Shown are gray-scale plots of the surface density in an  $(r - \varphi)$ -coordinate system.

2000; Snellgrove et al. 2001; Nelson & Papaloizou 2002) that during the early evolution, when the planets are still embedded in the disk, different migration speeds may lead to an approach of neighboring planets and eventually to resonant capture. More specifically, the evolution of planetary systems into a 2:1 resonant configuration was seen in the calculations of Kley (2000) prior to the discovery of any such systems.

In addition to hydrodynamic disk-planet simulations, many authors have analyzed the evolution of multiple-planet systems with N-body methods. Each of the known resonant systems have been considered in detail. Ji et al. (2002) and Lee & Peale (2002a) have modeled the evolution of 2:1 resonant system GJ 876, while the 3:1 system 55 Cnc has been analyzed by Ji et al. (2003b) and Lee & Peale (2002b), and the 2:1 system HD 82943 by Goździewski & Maciejewski (2001) and Ji et al. (2003a). Based on orbit integrations, these papers confirm that the planets in these systems are in resonance with each other. The dynamics and stability of resonant planetary systems in general has been recently studied by Beauge et al. (2002).

Here we present numerical calculations treating the evolution of two planets still embedded in a protoplanetary disk. We use both hydrodynamical simulations and simplified N-body integrations to follow the evolution of the system. In the first approach, the disk is evolved by solving the full time-dependent Navier-Stokes equations simultaneously with the evolution of the planets. Here, the motion of the planets is determined by the gravitational action of both planets, the star, and the disk. In the latter approach, we take a simplified approximation and perform 3-body (star plus two planets) calculations augmented by additional (damping) forces which approximately account for the gravitational influence of the disk (e.g. Lee & Peale 2002a). Using both approaches, allows a direct comparison of the alternative methods, and does enable us to determine the damping parameters required for the simpler (and much faster) second type of approach.

## 5.1. Observations

The basic orbital parameters of the three known systems in mean motion resonance are presented in Table 1. The orbital parameters for Gl 876 are taken from the dynamical fit of Laughlin & Chambers (2001), and for HD 82943 from Goździewski & Maciejewski (2001). Due to the uncertainty in the inclinations of the systems,  $M \sin i$ , rather than the exact mass of each planet, is listed. By including the mutual perturbations of the planets into their fit of Gl 876, Laughlin & Chambers (2001), however, are able to constraint that system's inclination to  $\sim 30^\circ - 50^\circ$ .

Two of the systems, Gl 876 and HD 82943, are in a nearly exact 2:1 resonance. We note that in both



Table 1. The orbital parameters of the three systems known to contain a mean motion resonance.  $P$  denotes the orbital period,  $M \sin i$  the mass of the planets,  $a$  the semi-major axis,  $e$  the eccentricity, and  $\varpi$  the angle of periastron. It should be noted that the orbital elements for shorter period planets undergo secular time variations. Thus in principle one should always state the epoch corresponding to these osculating elements (see e.g. Laughlin & Chambers 2001).

Name	P [d]	$M \sin i$ [ $M_{Jup}$ ]	$a$ [AU]	$e$	$\varpi$ [deg]
G1 876	(2:1)				
c	30.1	0.56	0.13	0.24	159
b	61.02	1.89	0.21	0.04	163
HD 82943	(2:1)				
b	221.6	0.88	0.73	0.54	138
c	444.6	1.63	1.16	0.41	96
55 Cnc	(3:1)				
b	14.65	0.84	0.11	0.02	99
c	44.26	0.21	0.24	0.34	61
d	5360	4.05	5.9	0.16	201

cases the outer planet is more massive, in one case by a factor of about two (HD 82943) and in the other by more than three (G1 876). The eccentricity of the inner (less massive) planet is larger than that of the outer one in both systems. For the system G1 876 the alignment of the orbits is such that the two periastrae are pointing in nearly the same direction. For the system HD 82943 these data have not been clearly identified, due to the much longer orbital periods, but they do not seem to be very different from each other. The third system, 55 Cnc, is actually a triple system. Here the inner two planets orbit the star very closely and are in a 3:1 resonance, while the third, most massive planet orbits at a distance of several AU.

## 5.2. Modeling resonant planets

The set of coupled hydrodynamical-N-body models presented in this contribution are calculated in the same manner as the models described above and in Kley (1998, 1999) for single planets and in Kley (2000) for multiple planets. The reader is referred to those papers for details on the computational aspects of the simulations. Other similar models, following explicitly the motion of single and multiple planets in disks, have been presented by Nelson et al. (2000), Bryden et al. (2000), and Snellgrove et al. (2001).

The initial hydrodynamic structure of the disk, which extends radially from  $r_{min}$  to  $r_{max}$ , is axisymmetric with respect to the location of the star, and the surface density scales as  $\Sigma(r) = \Sigma_0 r^{-1/2}$ , with superimposed initial gaps (Kley 2000). The initial velocity is pure Keplerian rotation ( $v_r = 0, v_\varphi = GM_*/r^{1/2}$ ). Here, we assume a fixed temperature law with  $T(r) \propto r^{-1}$  which follows from the assumed constant vertical height  $H/r = 0.10$ . The kinematic viscosity  $\nu$  is parameterized by an  $\alpha$ -description  $\nu =$

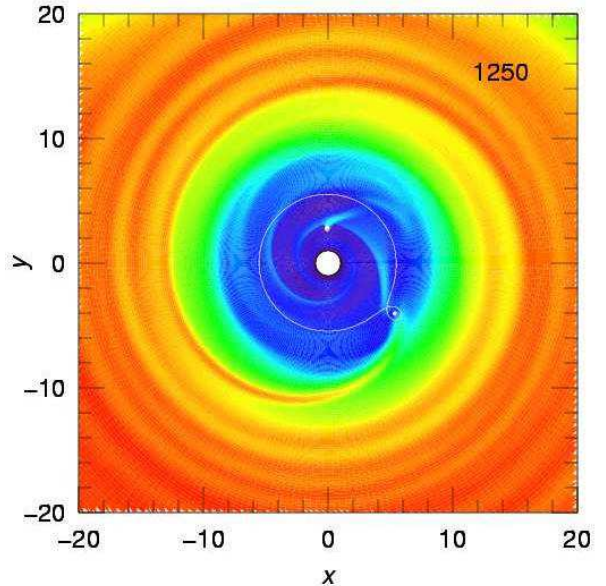


Figure 10. Overview of the density distribution after 1250 orbital periods of the inner planet. Higher density regions are brighter and lower ones are darker. The star lies at the center of the white inner region bounded by  $r_{min} = 1$  AU. The location of the two planets is indicated by the white dots, and their Roche-lobes are also drawn. Clearly seen are the irregular spiral wakes generated by the planets. Regular intertwined spiral arms are seen only outside of the second planet.

$\alpha c_s H$ , with the sound speed  $c_s = H v_\varphi / r$ .

In case of the simplified N-body computations, we follow the approach of Lee & Peale (2002a) and parameterize the imposed damping by specifying a damping rate  $a/\dot{a}$  for the outer planet only, as this is the only planet still in contact with the disk. This value may depend on time, taking the disk dissipation into account. The eccentricity damping time scale is a fixed fraction  $K$  of the semi-major axis damping, i.e.  $e/\dot{e} = K a/\dot{a}$ . Thus, in this case only a 3 body system (star and two planets) is followed by numerical integration, while the effects of the disk are taken into account simply through imposed additional forces reflecting the damping of  $a$  and  $e$ .

## 5.3. Results

At the start of the simulations both planets are placed into an axisymmetric disk at  $a_1 = 4$  and  $a_2 = 10$  AU, where the density is initialized with partially opened gaps superimposed on an otherwise smooth radial density profile. Upon starting the evolution the two main effects are:

- a) Because of the accretion of gas onto the two planets the radial region in between them is depleted in mass and finally cleared. This phase

typically takes only a few hundred orbital periods. At the same time the region interior to the inner planet loses material due to accretion onto the central star. Thus, after an initial transient phase we typically expect the configuration of two planets orbiting within an inner cavity of the disk, as seen in Fig.10, see also Kley (2000).

- b) After initialization, the planets quickly (within a few orbital periods) excite non-axisymmetric disturbances, viz. the spiral waves, in the disk. In contrast to the single planet case these are not stationary in time, because there is no preferred rotating frame. The gravitational torques exerted on the two planets by those density perturbations induce a migration process for the planets.

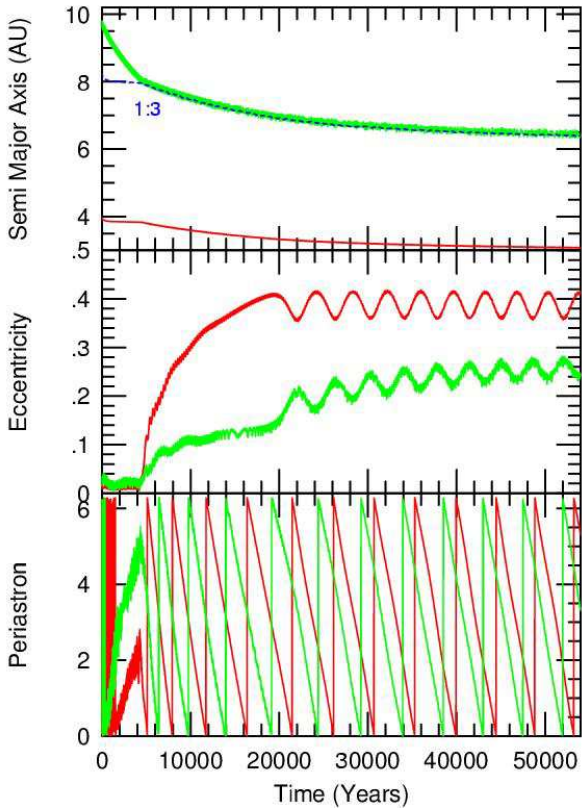


Figure 11. The semi-major axis ( $a$ ), eccentricity ( $e$ ) and position angle of the orbital periastron ( $\varpi$ ) for the two planets versus time. In this example, the planets have fixed masses of 3 and 5  $M_{Jup}$ , and are placed initially at 4 and 10 AU, respectively. The inner planet is denoted by the black line, the outer by the light gray line. The dotted reference line (labeled 3:1), indicates the location of the 3:1 resonance with respect to the inner planet.

Now, the planets' relative positions within the cavity have a distinct influence on their subsequent evolution. As a consequence of the clearing process, the inner planet is no longer surrounded by any disk material and thus cannot grow any further in mass. In addition, it cannot migrate anymore, because there

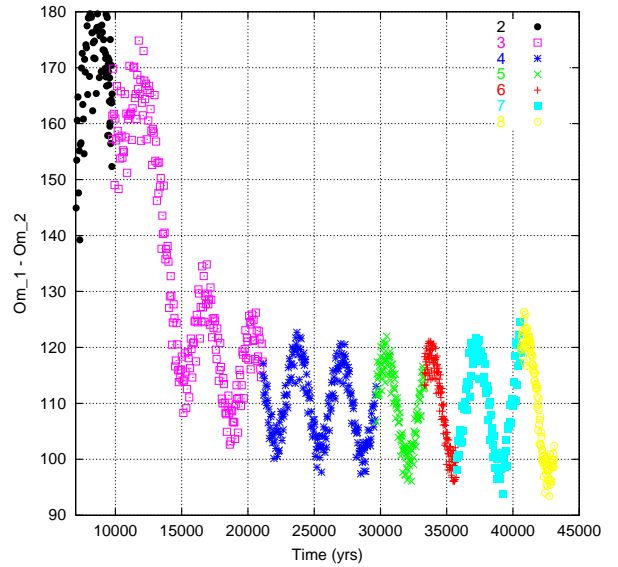


Figure 12. The evolution of the difference in periastron ( $\Delta\varpi = \varpi_2 - \varpi_1$ ) vs time for the two planets.

is no torque-exciting material left in its vicinity. All the material of the outer disk is still available, on the other hand, to exert negative (Lindblad) torques on the outer planet. Hence, in the initial phase of the computations we observe an inwardly migrating outer planet and a stalled inner planet with a constant semi-major axis (see the first 5000 yrs in the top panel of Fig.11).

This decrease in separation between the planets increases their gravitational interactions. Once the ratio of the planets' orbital periods has reached a ratio of two integers, i.e. they are close to a mean motion resonance, resonant capture of the inner planet by the outer one may ensue. Whether or not this does actually happen depends on the physical conditions in the disk (e.g. viscosity) and the orbital parameters of the planets. If the migration speed is too large, for example, there may not be enough time to excite the resonance, and the outer planet will continue migrating inward (e.g. Haghighipour 1999). Also, if the initial eccentricities are too small, then there may be no capture, particularly for second-order resonances such as the 3:1 resonance (see e.g. Murray & Dermott 1999). The typical time evolution of the semi-major axis ( $a$ ), eccentricity ( $e$ ) and direction of the periastron ( $\varpi$ ) are displayed in Fig.11. The planets were initialized with zero eccentricities at distances of 4 and 10 AU in a disk with partially cleared gaps.

In the beginning, after the inner gap has completely cleared, only the outer planet migrates inward, and the eccentricities of both planets remain relatively small, ( $\lesssim 0.02$ ). After about 5000 yrs the outer planet has reached a semi-major axis with an orbital period three times that of the inner planet. The periodic gravitational forcing leads to the capture of



the inner planet into a 3:1 resonance with the outer one. This is indicated by the dotted reference line (labeled 3:1) in the top panel of Fig.11, which marks the location of the 3:1 resonance with respect to the inner planet.

We summarize the following important features of the evolution after resonant capture:

- a) In the course of the subsequent evolution, the outer planet, which is still driven inward by the outer disk material, forces the inner planet to also migrate inwards. Both planets migrate inward simultaneously, always retaining their resonant configuration. Consequently, the migration speed of the outer planet slows down, and their radial separation declines.
- b) Upon resonant capture the eccentricities of both planets grow initially very fast before settling into an oscillatory quasi-static state which changes slowly on a secular time scale. This slow increase of the eccentricities on the longer time scale is caused by the growing gravitational forces between the planets, due to the decreasing radial distance of the two planets on their inward migration process.
- c) The ellipses/periastrae of the planets rotate at a constant, retrograde angular speed  $\dot{\varpi}$ . Coupled together by the resonance, the apsidal precession rate  $\dot{\varpi}$  for both planets is identical, which can be inferred from the parallel lines in the bottom panel of Fig.11. The orientation of the orbits is phase-locked with a constant separation  $\Delta\varpi = \varpi_2 - \varpi_1$ . The rotation period of the ellipses (apsidal lines) is slightly longer than the oscillation period of the eccentricities.

The capture into resonance and the subsequent libration of the orbits is illustrated further in Fig.12. As suggested in Fig.11 (bottom panel) the periastrae begin to align upon capture in the 3:1 resonance. Initially, during the phase when the eccentricities are still rising (between 5 and 20 thousand yrs), the difference of the periastrae settles intermediately to  $\Delta\varpi \approx 180^\circ$ . Then, upon saturation after about 20,000 yrs, the system re-adjusts and eventually establishes itself at  $\Delta\varpi \approx 107^\circ$ , with a libration amplitude of about  $7^\circ$ . This behaviour can be understood by an analysis of the interaction Hamiltonian for resonant systems (Beauge et al. 2002). By minimizing the interaction energy, the equilibrium values for  $\Delta\varpi$  (and  $\Theta_1$ , see below) can be obtained as a function of the mass and eccentricity of the two planets.

#### 5.4. Damped N-body computations

To illustrate the strengths of a simplified N-body computation we display in Fig.13 the eccentricity evolution of the full hydro and the damped 3-body

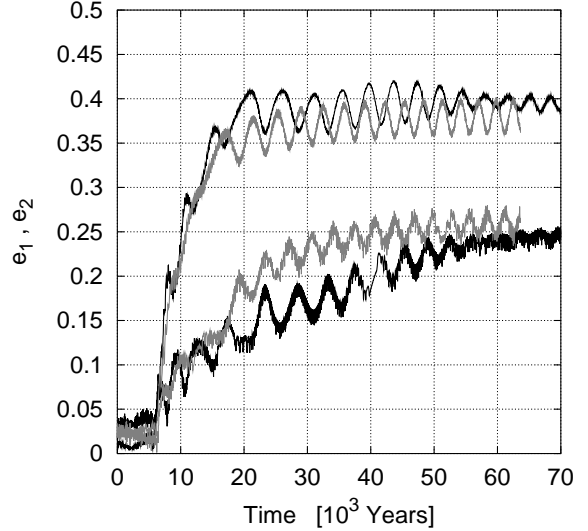


Figure 13. The evolution of the eccentricities of the inner planet (upper curves) and the outer planet (lower curves) for the full hydro model (black curves covering the whole time range) and a simplified damped N-body model (light gray), using a damping constant of  $K = 2.5$ .

case. Despite some differences which we attribute to the unknown eccentricity damping mechanism, the overall agreement is reasonable. For a given semi-major axis damping rate, the final values obtained for  $e_1$  and  $e_2$  at larger times depend on the initial values for the eccentricities and the amount of eccentricity damping. In this case we used an initial  $e(t_0) = 0.01$  for both planets and an eccentricity damping factor  $K = 2.5$ , i.e. a slightly shorter damping time scale for eccentricity as for semi-major axis. For all models we find that the eccentricity damping rate is of the same order as the semi-major axis damping, i.e.  $K = \mathcal{O}(1)$ . This finding is in contrast to Lee & Peale (2002a) who determined a much shorter eccentricity damping time, based on models for GJ 876.

#### 5.5. Resonant angles

To investigate the mass dependence of the resonant capture process we ran a sequence of damped N-body models with identical initial conditions but different masses. The results in terms of the resonant angle  $\Delta\varpi = \varpi_2 - \varpi_1$  are displayed in Fig.14. For small masses  $M_p < 2M_{Jup}$  we find capture occurs only into the 2:1 resonance. The low masses do not allow for a sufficiently strong interaction at the 3:1 resonance, and the outer planet migrates through that point. All 2:1 resonances settle into the complete symmetric configuration  $\Delta\varpi = \Theta_1 = 0$  (Fig.14). For the 2:1 resonance  $\Theta_1 = 2\lambda_2 - \lambda_1 - \varpi_1$ , where  $\lambda_i$  denotes the mean longitudes of the planets.

For the 3:1 resonances we see anti-symmetric config-

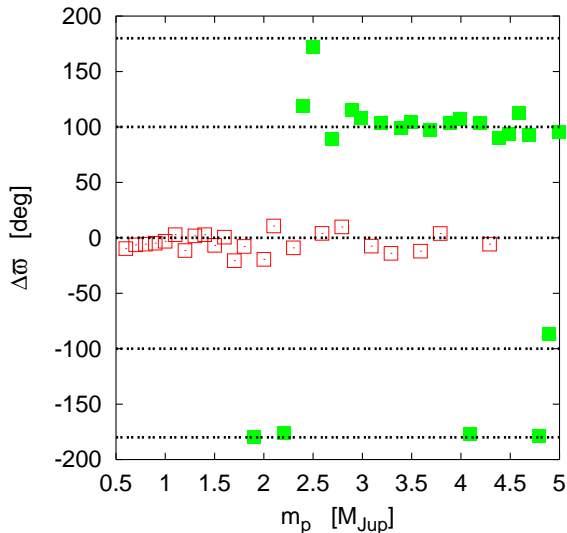


Figure 14. Results of a sequence of damped  $N$ -body simulations. Plotted is the difference of the periastrae  $\Delta\varpi = \varpi_2 - \varpi_1$  of the two planets after capture into resonance versus planet mass, where  $m_p = m_2 = m_1$ . The diamonds indicate capture in 2:1 resonance, while the plus signs are for 3:1 resonance. The other parameters are fixed, as described in the text. The horizontal lines indicate values of 0,  $\pm 100^\circ$  and  $\pm 180^\circ$ .

urations with anti-aligned periastrae,  $|\Delta\varpi| = 180^\circ$  and  $\Theta_1 = 0$  for masses around  $m_p = 2M_{Jup}$ , (when the first 3:1 cases begin to occur), while for all larger masses we find preferentially the previous non-symmetric configurations, where  $\Delta\varpi \approx 110^\circ$  and  $|\Theta_1| \approx 145^\circ$ . Here, for the case of 3:1 resonance,  $\Theta_1 = 3\lambda_2 - \lambda_1 - 2\varpi_1$ . As mentioned above, this behaviour may be an indication of a bifurcation in the stability properties of resonant systems, as claimed by Beauge et al. (2002). With additional damped  $N$ -body calculations we also find that systems entering a 5:2 resonance (not shown) exhibit a typical anti-symmetric behavior  $|\Delta\varpi| = 180^\circ$  and  $\Theta_1 = 0^\circ$ .

## 6. DISCUSSION

Through high resolution numerical computations of planets still embedded in protoplanetary disks it is possible to calculate the accretion migration rate of planets for the whole mass range from a few earth masses to over 1 Jupiter mass. The inferred timescales can be significantly shorter than the typical lifetimes of the disk.

Thus, we arrive at the problem of stopping the migration close to the stars, as well as for Jupiter in our own solar systems. In the case of the close-in planets it is believed that tidal interaction with the central star possibly through magnetic fields may be responsible for braking the planet. In the case of the solar system, early dissipation of the solar neb-

ula must have occurred to prevent the planets from moving further in.

Even though a lot of progress has been achieved during the last years, several problems will have to be addressed in the future. Among those are inclined orbits which may lead to disk warping (see  $\beta$  Pic disk), the inclusion of radiative transport to study observational effects, planets in binaries to investigate the constraints on the formation. The study of turbulent (MHD) and radiative disks has just begun and possibly will lead in the future to a change of some aspects of the migration and evolution scenario of young planets.

## REFERENCES

- Béjar, V. J. S., Martín, E. L., Zapatero Osorio, M. R., et al. 2001, *ApJ*, 556, 830
- Bate, M. R., Lubow, S. H., Ogilvie, G. I., & Miller, K. A. 2003, *MNRAS*, 341, 213
- Beauge, C., Ferraz-Mello, S., & Michtchenko, T. A. 2002, astro-ph/0210577, *ApJ*, submitted
- Bryden, G., Chen, X., Lin, D. N. C., Nelson, R. P., & Papaloizou, J. C. B. 1999, *ApJ*, 514, 344
- Bryden, G., Różyczka, M., Lin, D. N. C., & Bodenheimer, P. 2000, *ApJ*, 540, 1091
- D’Angelo, G., Henning, T., & Kley, W. 2002, *A&A*, 385, 647
- D’Angelo, G., Kley, W., & Henning, T. 2003, *ApJ*, 586, 540
- de la Fuente Marcos, C. & Barge, P. 2001, *MNRAS*, 323, 601
- Dreizler, S., Hauschildt, P. H., Kley, W., et al. 2003, *A&A*, 402, 791
- Goździewski, K. & Maciejewski, A. J. 2001, *ApJ*, 563, L81
- Godon, P. & Livio, M. 2000, *ApJ*, 537, 396
- Haghighipour, N. 1999, *MNRAS*, 304, 185
- Ji, J., Kinoshita, H., Liu, L., Guangyu, L., & Nakai, H. 2003a, in Proceedings of IAU 189 Colloquium, Sept. 2002, Nanjing, P.R. China, in press, astro-ph/0301353
- Ji, J., Kinoshita, H., Liu, L., & Li, G. 2003b, *ApJ*, 585, L139
- Ji, J., Li, G., & Liu, L. 2002, *ApJ*, 572, 1041
- Klahr, H. H. & Bodenheimer, P. 2003, *ApJ*, 582, 869
- Kley, W. 1998, *A&A*, 338, L37
- . 1999, *MNRAS*, 303, 696
- . 2000, *MNRAS*, 313, L47
- Kley, W., D’Angelo, G., & Henning, T. 2001, *ApJ*, 547, 457
- Kokubo, E. & Ida, S. 1998, *Icarus*, 131, 171
- Konacki, M., Torres, G., Jha, S., & Sasselov, D. D. 2003, *Nature*, 421, 507
- Laughlin, G. & Chambers, J. E. 2001, *ApJ*, 551, L109

- Lee, M. H. & Peale, S. J. 2002a, *ApJ*, 567, 596
- Lee, M. H. & Peale, S. J. 2002b, in *Scientific Frontiers in Research on Extrasolar Planets*, ASP Conference Series, in press, astro-ph/0209176
- Lin, D. N. C. & Papaloizou, J. 1980, *MNRAS*, 191, 37
- Lin, D. N. C. & Papaloizou, J. C. B. 1993, in *Protostars and Planets III*, 749–835
- Lissauer, J. J. 1993, *ARA&A*, 31, 129
- . 2002, *Nature*, 419, 355
- Lubow, S. H., Seibert, M., & Artymowicz, P. 1999, *ApJ*, 526, 1001
- Lucas, P. W. & Roche, P. F. 2000, *MNRAS*, 314, 858
- Marcy, G. W., Fischer, D. A., Butler, R. P., & Vogt, S. S. 2003, in *Space Science Reviews*, in press
- Mazeh, T. & Zucker, S. 2002, *Reviews of Modern Astronomy*, 15, 133
- Murray, C. D. & Dermott, S. F. 1999, *Solar system dynamics* (Solar system dynamics by Murray, C. D., 1999)
- Nelson, R. P. & Papaloizou, J. C. B. 2002, *MNRAS*, 333, L26
- Nelson, R. P., Papaloizou, J. C. B., Masset, F. . . , & Kley, W. 2000, *MNRAS*, 318, 18
- Papaloizou, J. C. B. & Nelson, R. P. 2003, *MNRAS*, 339, 983
- Santos, N. C., Israelian, G., Mayor, M., Rebolo, R., & Udry, S. 2003, *A&A*, 398, 363
- Sasselov, D. D. & Lecar, M. 2000, *ApJ*, 528, 995
- Snellgrove, M. D., Papaloizou, J. C. B., & Nelson, R. P. 2001, *A&A*, 374, 1092
- Tanaka, H., Takeuchi, T., & Ward, W. R. 2002, *ApJ*, 565, 1257
- Thommes, E. W., Duncan, M. J., & Levison, H. F. 2003, *Icarus*, 161, 431
- Ward, W. R. 1997, *Icarus*, 126, 261